Four-view Geometry with Unknown Radial Distortion*

Petr Hruby
ETH Zürich
Dept. of Computer Science
petr.hruby@inf.ethz.ch

Viktor Korotynskiy
CIIRC, CTU in Prague
viktor.korotynskiy@cvut.cz

Timothy Duff
University of Washington
timduff@uw.edu

Luke Oeding
Auburn University
oeding@auburn.edu

Marc Pollefeys
ETH Zürich
Dept. of Computer Science
marc.pollefeys@inf.ethz.ch

Tomas Pajdla
CIIRC, CTU in Prague
pajdla@cvut.cz

Viktor Larsson
Lund University
viktor.larsson@math.lth.se

Abstract

We present novel solutions to previously unsolved problems of relative pose estimation from images whose calibration parameters, namely focal lengths and radial distortion, are unknown. Our approach enables metric reconstruction without modeling these parameters. The minimal case for reconstruction requires 13 points in 4 views for both the calibrated and uncalibrated cameras. We describe and implement the first solution to these minimal problems. In the calibrated case, this may be modeled as a polynomial system of equations with 3584 solutions. Despite the apparent intractability, the problem decomposes spectacularly. Each solution falls into a Euclidean symmetry class of size 16, and we can estimate 224 class representatives by solving a sequence of three subproblems with 28, 2, and 4 solutions. We highlight the relationship between internal constraints on the radial quadrifocal tensor and the relations among the principal minors of a 4×4 matrix. We also address the case of 4 upright cameras, where 7 points are minimal. Finally, we evaluate our approach on simulated and real data and benchmark against previous calibration-free solutions, and show that our method provides an efficient startup for an SfM pipeline with radial cameras.

*Supported by EU RDF IMPACT No. CZ.02.1.01/0.0/0.0/15 003/0000468 and EU H2020 No. 871245 SPRING projects. Viktor Larsson was funded by the strategic research project ELLIIT. Timothy Duff acknowledges support from an NSF Mathematical Sciences Postdoctoral Research Fellowship (DMS-2103310). Viktor Korotynskiy was partially supported by the Grant Agency of CTU in Prague project SGS23/056/OHK3/1T/13.

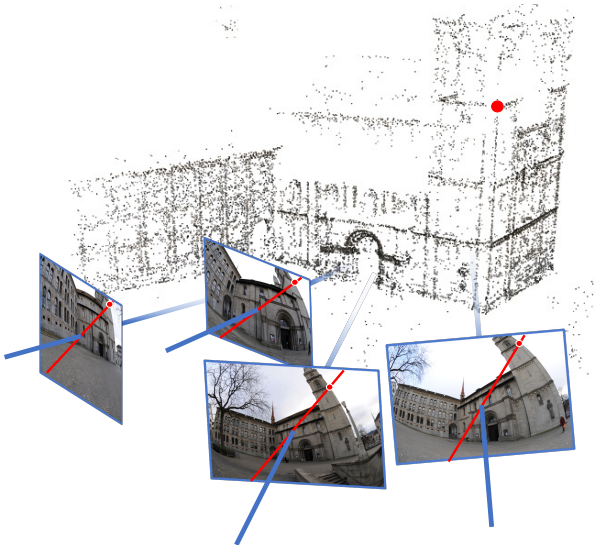

Figure 1. **Four-view Structure-from-Motion with 1D radial cameras.** A radial camera projects a 3D point onto a radial line passing through its pinhole projection.

1. Introduction

Determining the relative position and orientation of two or more cameras is a classical problem in computer vision [33]. It appears in the back-end of many vision systems, usually to initialize SLAM [54] or further reconstruction in Structure-from-Motion [70]. Much effort has been concentrated on the development of methods for 3D reconstruction using perspective cameras with various additional lens distortion models [1, 52, 70].

1.1. Motivation

Any type of geometric estimation usually requires knowing the intrinsic calibration, i.e., the mapping from pixels in the image to the directions of the incoming viewing rays. If the intrinsic parameters are unknown, so-called *self-calibration* [26] can be attempted where the camera extrinsic and intrinsic calibration are jointly estimated. Historically, this is done in a stratified approach where a projective reconstruction is first obtained followed by a metric upgrade step [33]. These approaches are usually limited in the complexity of the cameras that can be handled; often making the assumption of pure pinhole projection.

An orthogonal line of work aims to recover camera extrinsics without estimating intrinsics. Assuming that the camera is radially symmetric (unit aspect ratio and distortion that only varies radially), it is possible to extract geometric constraints on camera poses that are invariant to focal length or radial distortion. The idea, first introduced by Tsai [78], is to only consider the angle and ignore the radius for each projection, essentially projecting 3D points onto radial lines in the image. Enforcing that the radial line pass through the 2D keypoint then yields a geometric constraint on both the 3D point and the camera pose (excluding the pure forward translation). In this context, the camera (mapping from 3D point to radial line) is referred to as a *1D radial camera* [47, 76]. Mathematically, this gives a perspective camera from $\mathbb{P}^3$ to $\mathbb{P}^1$, illustrated in Figure 1.

Radial cameras bring an important alternative to classical uncalibrated (radially distorted) pinhole cameras. With radial cameras, we can completely avoid (auto-)calibrating complicated radial distortion models (and focal lengths) of all cameras involved, just by using 4 instead of 2 cameras in 3D reconstruction initialization.

1.2. Contribution

Motivated by the 1D radial construction above, we study problems from the multi-view geometry of $\mathbb{P}^3 \dashrightarrow \mathbb{P}^1$ cameras. In particular, we consider problems containing four images (the minimum number where constraints can be obtained in a general configuration). Solving these problems allows us to effectively perform metric reconstruction for cameras with unknown radial distortion under very weak assumptions on the distortion, namely that it is radially symmetric and centered in the image.

We provide three main technical contributions. First, we formulate 13-point calibrated minimal problem for 4 radial cameras and, guided by computational Galois theory, show that this (seemingly) hard problem with 3584 complex solutions decomposes into subproblems with 28, 2, and 4 solutions, among which the minimal case for uncalibrated cameras also appears. We present a parallel study for the 7-point minimal problem for upright radial cameras. Secondly, we present the internal constraints on the radial quadrifocal tensor and show that they are given by non-trivial relations among the principal minors of a 4×4 matrix derived in [39, 53, 55]. Finally, based on the previous theoretical contributions, we design and implement stable and practical (78 & 18 ms runtime) Homotopy Continuation (HC) minimal solvers and show their quality in simulated and real experiments. We show that our solvers provide efficient initialization of the radial camera 3D reconstruction pipeline [47]. This provides previously missing piece for building an efficient radial camera 3D reconstruction pipelines.

Camera model		Method	# cam.	# pts
$\mathbb{P}^2 \dashrightarrow \mathbb{P}^3$	Uncalibrated	Linear [34]	2	8
	Uncalibrated	Minimal [38]	2	7
	Calibrated	Minimal [58]	2	5
	Upright	Minimal [29]	2	3
$\mathbb{P}^1 \dashrightarrow \mathbb{P}^1$	Uncalibrated	Linear / Minimal [75]	3*	7
	Calibrated	Minimal [47]	3*	6
$\mathbb{P}^3 \dashrightarrow \mathbb{P}^1$	Uncalibrated	Linear [75]	4	15
	Uncalibrated	Minimal [**OURS**]	4	13
	Calibrated	Minimal [**OURS**]	4	13
	Upright	Minimal [**OURS**]	4	7

* Requires intersecting principal axis or planar scene.

Table 1. Comparison between relative pose solvers. **OURS** include the first minimal solvers for general 1D radial cameras.

2. Related work

One of our contributions is to fill a gap in the vision literature by describing and implementing, for the first time, minimal solutions for radial camera relative pose in the uncalibrated, calibrated, and upright cases. To put our work in context, we present in Table 1 a comparison with methods for relative pose estimation in the classical case of cameras $\mathbb{P}^3 \dashrightarrow \mathbb{P}^2$ as well as the radial cameras $\mathbb{P}^3 \dashrightarrow \mathbb{P}^1$ studied here. We also note that there are several works studying the multifocal constraints and minimal problems associated to cameras $\mathbb{P}^2 \dashrightarrow \mathbb{P}^1$, including [17, 27, 49, 65, 66, 69]. Notably, the existence of inequivalent projective reconstructions for cameras $\mathbb{P}^2 \dashrightarrow \mathbb{P}^1$ was observed in [65]. This observation was generalized to cameras $\mathbb{P}^n \dashrightarrow \mathbb{P}^1$ using the formalism of Grassmann tensors [31, 32]. Initial studies of quadrifocal tensors appeared in [72],[33, Ch. 17], and radial multifocal tensors were introduced in [75]. A connection between a flat-landers's quadrifocal tensor and principal minors was made in [59], which also studied the relations on quadrifocal tensors. Equations for the radial quadrifocal tensor were explicitly described in [48], and some of these relations were discovered in 1897, in work of Nanson [55].

Minimal problems and their solvers play an outsized role in structure-from-motion and other geometric problems from vision [5, 6, 11, 12, 23, 24, 40, 43, 44, 51, 56, 64, 68, 79].

For our purposes, a *minimal problem* is a system of equations that is polynomial in both measurements and certain unknown quantities, and which has an exact solution for generic, random, or noisy measurements. The inherent difficulty of solving polynomial systems of equations presents a challenge for developing minimal solvers. For many tasks, state-of-the art methods [6, 46, 50] based on symbolic computation offer efficient and stable solutions suitable for use within RANSAC [28, 67].

A common element shared by many minimal solvers is that they first compute all solutions over the *complex numbers* $\mathbb{C}$, despite the fact that only real solutions are of interest. They also often exploit a key property of any minimal problem: namely, that the number of complex solutions is constant over a dense subset of the space of measurements. This property is also often exploited by *homotopy continuation (HC)* methods, which have been applied to problems from vision in several recent works [8, 14, 19–21, 24, 25, 36, 40, 42].

Two major obstacles to solving any minimal problem are 1. when the number of complex solutions is too large, and 2. when the polynomials themselves are too large. To get around the first obstacle, a "pick & solve" framework from recent work [40] proposes picking one HC start solution with a shallow neural network. This approach was observed to give runtimes suitable for RANSAC for certain tasks. Its main drawback is that the method is inherently local, and will likely fail for a large proportion of RANSAC samples. In contrast, tracking all HC paths over the complex numbers is *globally convergent with probability-one* [73, Thm. 7.1.1], and may be viable for problems where symbolic solutions are lacking. We offer a substantial contribution towards the challenge of improving the performance of HC when applied to these problems.

The second obstacle mentioned above is also relevant to our work. As we explain in Section 4, the internal constraints of radial quadrifocal tensors are characterized by 718 polynomial equations of degree 12. This presents a challenge to approaches based on symbolic computation. However, with the appropriate setup, HC methods allow us to work with only two of these equations.

Another important consideration is that minimal problems sometimes decompose into minimal subproblems or possess various symmetries. A classical example of is that of the five point problem, which decomposes as essential matrix estimation followed by recovering a "twisted pair" of camera matrices. Automatic detection of special classes of symmetries is addressed in works such as [3, 45]. In general, decomposition of a minimal problem can be detected from its *Galois group*, which can be heuristically computed with HC [21, 37]. For the problems treated in this paper, knowledge of the Galois group led us to discover various algebraic simplifications. For 13 points in 4 views, we witness a dramatic simplification—3584 solutions in calibrated camera matrices can be reduced to just 28 solutions in quadrifocal tensors. Correspondingly, our minimal solver computes 28 solutions by tracking 28 HC paths, after which results are lifted to camera matrices by solving equations of smaller degree. Moreover, the Galois group contains the symmetric group S_{28} as a subgroup, indicating that our approach is *algebraically optimal* (cf. [4, 57].) Similarly, for the 7-point problem the Galois group contains S_{25}, and we track an algebraically optimal 25 paths.

Our work shows that minimal estimation of the radial quadrifocal tensor has a rich mathematical structure, which was useful for developing the solutions presented herein. However, understanding these connections is not necessary to use or implement the solvers themselves, which we describe in Section 5.

3. Problem formulations

Throughout, $\mathbb{P}^n$, or $\mathbb{P}(\mathbb{R}^{n+1})$, denotes the n-dimensional projective space over the field of real numbers $\mathbb{R}$. We use $\sim$ for equality up to a non-zero scale.

A *radial camera* [47, 75] may be defined to be a projective linear map $P : \mathbb{P}^3 \dashrightarrow \mathbb{P}^1$. Thus, a radial camera may be represented by a 2×4 camera matrix. Abusing notation, we may also denote such a matrix by P, but keeping in mind that any nonzero scalar multiple of P will represent the same map. Thus a radial camera $P \in \mathbb{P}(\mathbb{R}^{2\times 4})$ has $2 \times 4 - 1 = 7$ degrees of freedom.

The radial camera P associates a world point in $\mathbb{P}^3$ with the *radial line* passing through the center of distortion in an image and the projection of the world point under the usual pinhole model. The center of distortion may be assumed to be $[0 : 0 : 1] \in \mathbb{P}^2$, so that the equation of the radial line is parametrized by the projected image point $[u : v : 1] \in \mathbb{P}^2$ as a direction vector, thus giving a point $\mathbf{l} = [u : v] \in \mathbb{P}^1$. With these assumptions, a pinhole camera $P_{\text{pin}} : \mathbb{P}^3 \dashrightarrow \mathbb{P}^2$ can be associated with a radial camera P as follows:

$$P = \begin{bmatrix} 1 & 0 & 0 \\ 0 & 1 & 0 \end{bmatrix} \cdot P_{\text{pin}}. \tag{1}$$

Suppose we image n points in $\mathbb{P}^3$ with four radial cameras P_1, P_2, P_3, P_4, so that for each $k = 1, \ldots, n$ we obtain a correspondence $\mathbf{l}_{1k}, \ldots, \mathbf{l}_{4k} \in \mathbb{P}^1$. Representing each $\mathbf{l}_{ik}$ as a 2×1 vector, we have correspondence constraints

$$\det \begin{bmatrix} P_1 & \mathbf{l}_{1k} & \mathbf{0} & \mathbf{0} & \mathbf{0} \\ P_2 & \mathbf{0} & \mathbf{l}_{2k} & \mathbf{0} & \mathbf{0} \\ P_3 & \mathbf{0} & \mathbf{0} & \mathbf{l}_{3k} & \mathbf{0} \\ P_4 & \mathbf{0} & \mathbf{0} & \mathbf{0} & \mathbf{l}_{4k} \end{bmatrix} = 0, \quad k = 1, \ldots, n. \tag{2}$$

These equations are homogeneous in each P_i and $\mathbf{l}_{ik}$. The $2 \times 2 \times 2 \times 2$ *radial quadrifocal tensor* [75], defined by

$$T_{P_1,\ldots,P_4}[i, j, k, l] = (-1)^{i+j+k+l} \det \begin{bmatrix} P_1[i,:] \\ P_2[j,:] \\ P_3[k,:] \\ P_4[l,:] \end{bmatrix}, \tag{3}$$

gives the coefficients of a quadrilinear form $T_{P_1,\dots,P_4}$ on $(\mathbb{P}^1)^4$. Equation (2) becomes

$$T_{P_1,\dots,P_4}(\mathbf{l}_{1k},\mathbf{l}_{2k},\mathbf{l}_{3k},\mathbf{l}_{4k}) = 0, \quad k = 1,\dots,n. \tag{4}$$

For a given set of observations $\mathbf{l} \in (\mathbb{P}^1)^{4n}$, our task is to recover the camera matrices $(P_1,\dots,P_4)$ from n correspondences up to natural ambiguities.

3.1. 13-point uncalibrated relative pose

In the uncalibrated case, we seek to recover the camera matrices up to projective change of coordinates in the world. In other words, we want to recover the cameras $(P_1,\dots,P_4)$ up to the action of the projective linear group $\mathrm{PGL}_4(\mathbb{R}) = \{H \in \mathbb{P}(\mathbb{R}^{4\times 4}) \mid \det H \neq 0\}$. This group acts (on the right) as $H \cdot (P_1,\dots,P_4) = (P_1H,\dots,P_4H)$. Up to this group action, a generic 4-tuple of camera matrices can be brought to a standard form as in Eq. (5) below (see SM Proposition 2).

$$\begin{aligned} P_1 &= \begin{bmatrix} 1 & 0 & 0 & 0 \\ p_{11} & p_{11} & p_{11} & p_{11} \end{bmatrix}, \quad P_2 = \begin{bmatrix} 0 & 1 & 0 & 0 \\ p_{21} & p_{22} & p_{23} & p_{24} \end{bmatrix}, \\ P_3 &= \begin{bmatrix} 0 & 0 & 1 & 0 \\ p_{31} & p_{32} & p_{33} & p_{34} \end{bmatrix}, \quad P_4 = \begin{bmatrix} 0 & 0 & 0 & 1 \\ p_{41} & p_{42} & p_{43} & p_{44} \end{bmatrix}. \end{aligned} \tag{5}$$

For $n = 13$ equations (2) we have 13 unknowns, and we expect finitely many solutions. Indeed, Gröbner basis computations show that equations have 56 solutions over the complex numbers for generic data $\mathbf{l}_{ij}$. However, as previously observed in [32], four radial cameras are not uniquely determined by their radial quadrifocal tensor. With respect to the standard form (5), this 2-fold *Hartley-Schaffilitsky symmetry* is defined by

$$\begin{aligned} \mathrm{HS}(P_1) = P_1, \quad \mathrm{HS}(P_2) &= \begin{bmatrix} 0 & 1 & 0 & 0 \\ p_{21} & p_{22} & \frac{p_{21}p_{32}}{p_{31}} & \frac{p_{21}p_{42}}{p_{41}} \end{bmatrix}, \\ \mathrm{HS}(P_3) &= \begin{bmatrix} 0 & 0 & 1 & 0 \\ p_{31} & \frac{p_{31}p_{23}}{p_{21}} & p_{33} & \frac{p_{31}p_{43}}{p_{41}} \end{bmatrix}, \\ \mathrm{HS}(P_4) &= \begin{bmatrix} 0 & 0 & 0 & 1 \\ p_{41} & \frac{p_{41}p_{24}}{p_{21}} & \frac{p_{41}p_{34}}{p_{31}} & p_{44} \end{bmatrix}. \end{aligned} \tag{6}$$

This may be understood as a rational map

$$\begin{aligned} \mathrm{HS} : \mathbb{R}^{13} \dashrightarrow \mathbb{R}^{13}, \\ (P_1,\dots,P_4) \mapsto (\mathrm{HS}(P_1),\dots,\mathrm{HS}(P_4)), \end{aligned}$$

which defines a quadratic involution in the sense that $\mathrm{HS} \circ \mathrm{HS}$ equals the identity map for all points where it is defined. Additionally, cameras $(P_1,\dots,P_4)$ and $(\mathrm{HS}(P_1),\dots,\mathrm{HS}(P_4))$ determine the same radial quadrifocal tensor. See [65] for a similar symmetry for cameras $\mathbb{P}^2 \dashrightarrow \mathbb{P}^1$, and SM Eq. (30) for an alternate formula.

3.2. 13-point calibrated relative pose

We say a radial camera P is *calibrated* if Eq. (1) holds for some calibrated pinhole camera P_{pin}. That is, if there exists a matrix representing the radial camera of the form

$$P = \begin{bmatrix} \mathbf{r}_1^\top & t_1 \\ \mathbf{r}_2^\top & t_2 \end{bmatrix} \quad \text{with} \quad \mathbf{r}_1^\top \mathbf{r}_1 = \mathbf{r}_2^\top \mathbf{r}_2 = 1, \quad \mathbf{r}_1^\top \mathbf{r}_2 = 0. \tag{7}$$

The matrix P in (7) has $5 = 3 + 2$ degrees of freedom, as can be seen from the (truncated) Cayley parametrization of admissible $(\mathbf{r}_1^\top; \mathbf{r}_2^\top) \in \mathbb{R}^{2\times 3} \cong \mathbb{R}^6$, which is 1-1:

$$\begin{aligned} &\mathrm{Cay} : \mathbb{R}^3 \dashrightarrow \mathbb{R}^{2\times 3} \\ &(x,y,z) \mapsto \begin{bmatrix} \frac{1+x^2-(y^2+z^2)}{1+x^2+y^2+z^2} & \frac{2(xy-z)}{1+x^2+y^2+z^2} & \frac{2(xz+y)}{1+x^2+y^2+z^2} \\ \frac{2(xy+z)}{1+x^2+y^2+z^2} & \frac{1+y^2-(x^2+z^2)}{1+x^2+y^2+z^2} & \frac{2(yz-x)}{1+x^2+y^2+z^2} \end{bmatrix}. \end{aligned} \tag{8}$$

In the calibrated case, we seek to recover the camera matrices up to action of the similarity group,

$$\mathrm{S}(3) = \left\{ H \in \mathrm{PGL}_4(\mathbb{R}^{4\times 4}) \,\middle|\, H \sim \begin{bmatrix} R & \mathbf{t} \\ \mathbf{0}^\top & s \end{bmatrix}, \, R \in \mathrm{SO}_3(\mathbb{R}) \right\}. \tag{9}$$

Up to the $\mathrm{S}(3)$ action, we may assume the following standard form (see SM Proposition 3.)

$$\begin{aligned} P_1 = \begin{bmatrix} 1 & 0 & 0 & 0 \\ 0 & 1 & 0 & 0 \end{bmatrix}, \quad P_2 &= \left[\begin{array}{c|c} \mathrm{Cay}(x_2,y_2,z_2) & \mathbf{e}_2 \end{array} \right], \\ P_3 &= \left[\begin{array}{c|c} \mathrm{Cay}(x_3,y_3,z_3) & \mathbf{t}_3 \end{array} \right], \\ P_4 &= \left[\begin{array}{c|c} \mathrm{Cay}(x_4,y_4,z_4) & \mathbf{t}_4 \end{array} \right]. \end{aligned} \tag{10}$$

Once again, for $n = 13$ in Eq. (2), we have 13 equations in 13 unknowns: $x_i, y_i, z_i, \mathbf{t}_j, i = 2,3,4$, $j = 3,4$. Using monodromy to solve these equations (see eg. [18]), we find that they have 3584 solutions over the complex numbers. However, SM Proposition 4 shows that there is a group of 16 similarity transformations that preserve the set of solutions. To "collapse" the orbits of this order-16 symmetry group, we may consider an alternate formulation of the calibrated relative pose problem. The basic idea is to first solve the uncalibrated problem, and then perform a *metric upgrade* by estimating the *dual absolute quadric* [33, § 3.7]. The relevant ideas may be found in previous works such as [13,47,77]. Briefly, if $(P_1,\dots,P_4)$ is a 4-tuple of uncalibrated radial cameras, the main task is to compute a 4×4 symmetric matrix Q such that

$$\begin{aligned} P_k Q P_k^\top \sim I, \quad k = 1,\dots,4, \\ \det(Q) = 0. \end{aligned} \tag{11}$$

Having computed such a Q, the metric upgrade proceeds by computing an eigendecomposition

$$Q = V \,\mathrm{diag}(\lambda_1^2, \lambda_2^2, \lambda_3^2, 0) V^\top, \tag{12}$$

from which we obtain a *calibrating homography*

$$H = V \,\mathrm{diag}(\lambda_1, \lambda_2, \lambda_3, 1). \tag{13}$$

Proposition 1 (Metric upgrade, see SM Proposition 5)**.** If H in (13) has full rank, then all four transformed radial cameras $P_1H, \dots, P_4H$ are calibrated.

Thus, we may formulate the 13-point calibrated relative pose problem as solving the system of equations given by (2) and (11), with cameras P_k given as in (5). Imposing an additional affine-linear equation in Q to remove the scaling ambiguity, this gives us a system of a polynomial equations with $224 = 4 \cdot 56$ solutions. This system of equations has a "triangular" structure (cf. [10, § 2.3]): we can first solve the uncalibrated problem, then perform a metric upgrade for any resulting solution $(P_1, \dots, P_4) \in \mathbb{P}(\mathbb{R}^{2\times 4})^4$. This triangular structure is reflected in the Galois group—see SM Section 7.2 for details.

3.3. 7-point upright relative pose

For the upright case, take $x_i = z_i = 0$ in (10):

$$\begin{aligned} P_1(\mathbf{y},\mathbf{t}) &= \left[\begin{array}{c|c} \mathrm{Cay}(0,\,0,\,0) & \mathbf{0} \end{array}\right], \\ P_2(\mathbf{y},\mathbf{t}) &= \left[\begin{array}{c|c} \mathrm{Cay}(0,y_2,0) & \mathbf{e}_2 \end{array}\right], \\ P_3(\mathbf{y},\mathbf{t}) &= \left[\begin{array}{c|c} \mathrm{Cay}(0,y_3,0) & \mathbf{t}_3 \end{array}\right], \\ P_4(\mathbf{y},\mathbf{t}) &= \left[\begin{array}{c|c} \mathrm{Cay}(0,y_4,0) & \mathbf{t}_4 \end{array}\right]. \end{aligned} \tag{14}$$

Now, with only 7 unknowns, we expect that only 7 correspondences are needed. Indeed, we find that equations (2) now have only 50 complex solutions. Unlike the calibrated case, where we can reduce to the uncalibrated case as a subproblem, the decomposition into subproblems is less dramatic. However, one of the 15 nontrivial symmetries from the previous section, sending $y_i \mapsto -y_i$ and fixing translations, does specialize to the upright setting.

4. Internal constraints on quadrifocal tensors

Let us now describe internal constraints on radial quadrifocal tensors. We exploit non-trivial results from mathematical literature allowing us to arrive at a practical use of seemingly very complicated polynomial identities.

4.1. General and calibrated case

Consider the map that associates 4-tuples of radial camera matrices to their quadrifocal tensor:

$$\begin{aligned} \Psi : (\mathbb{P}^7)^4 &\dashrightarrow \mathbb{P}^{15}, \\ (P_1, \dots, P_4) &\mapsto T_{P_1,\dots,P_4}. \end{aligned}$$

By analogy with well-known constraints characterizing essential and fundamental matrices, the space of all valid quadrifocal tensors must satisfy various constraints given by polynomial equations. These constraints were studied in mathematics more than a century ago [53, 55], albeit in a different setting. Indeed, they can be understood as relations on the *principal minors* of a 4×4 matrix X. The study of relations among principal minors of various types of matrices is an active area of research in mathematics and computer science: see eg. [2, 39, 41, 48, 60].

To see the correspondence between radial quadrifocal tensors and 4×4 principal minors, note that by fixing four points in $\mathbb{P}^3$, our camera matrices may take the form

$$\begin{aligned} P_1 &= \left[\begin{smallmatrix} -1 & 0 & 0 & 0 \\ x_{11} & x_{12} & x_{13} & x_{14} \end{smallmatrix}\right], \quad P_2 = \left[\begin{smallmatrix} 0 & -1 & 0 & 0 \\ x_{21} & x_{22} & x_{23} & x_{24} \end{smallmatrix}\right], \\ P_3 &= \left[\begin{smallmatrix} 0 & 0 & -1 & 0 \\ x_{31} & x_{32} & x_{33} & x_{34} \end{smallmatrix}\right], \quad P_4 = \left[\begin{smallmatrix} 0 & 0 & 0 & -1 \\ x_{41} & x_{42} & x_{43} & x_{44} \end{smallmatrix}\right]. \end{aligned} \tag{15}$$

With cameras as in (15), the tensor entry $T_{P_1,\dots,P_4}[i,j,k,l]$ is equal to the subdeterminant of $X = (x_{ij})_{1\le i,j\le 4}$ obtained by selecting as rows and columns the positions of nonzero indices i, j, k, l. For example: the tensor entry $T_{P_1,\dots,P_4}[1,0,1,0]$ equals $A_{13}(X)$, the principal minor obtained by deleting rows 2 and 4 from X. Similarly, $T_{P_1,\dots,P_4}[0,1,1,1] = A_{234}(X)$, obtained by deleting row 1 from X. Under this correspondence, we see that the image of Ψ is the image of the *projective principal minor map*,

$$\begin{aligned} \Phi : \mathbb{R}^{4\times 4} &\dashrightarrow \mathbb{P}^{15}, \\ X &\mapsto \big[A_S(X) \mid S \subset \{1,2,3,4\}\big]. \end{aligned}$$

The image of the map Φ is a dense subset of a projective variety of dimension 13 and degree 28, which is cut out by 718 linearly independent homogeneous polynomials of degree 12. This accords with our minimal solver, which requires 13 correspondences and must track 28 HC paths. We refer to Section 7.3 for a detailed discussion.

Although 718 polynomials are needed to define the radial quadrifocal variety *globally*, only $2 = 15 - 13$ are needed to define it *locally* in a neighborhood of any generic radial quadrifocal tensor. As remarked eg. in [40, SM § 16], this means we only need 2 equations when running HC from a set of 28 meaningful start solutions. The two equations we use are defined in terms of the Nanson matrix $\mathbf{N}$—see SM Equation (29). Expressing the Nanson matrix in terms of T, we let $f_{\text{Nanson}}(T) = \det{}^h \mathbf{N}[1:4,:]$, and $g_{\text{Nanson}}(T) = \det{}^h \mathbf{N}[2:5,:]$, where $\bullet^h$ denotes homogenization ([16, § 8.2]) with respect to the variable $T_{0,0,0,0}$.

4.2. Upright case

Although calibration does not impose additional internal constraints on the radial quadrifocal tensor, the same cannot be said in the case of upright cameras. Here, we study equations vanishing on the image of the map

$$\begin{aligned} \Psi_{\text{up}} : \mathbb{R}^7 &\dashrightarrow \mathbb{P}^{15}, \\ (y_2, y_3, t_{31}, t_{32}, y_4, t_{41}, t_{42}) &\mapsto T_{P_1(\mathbf{y},\mathbf{t}),\dots,P_4(\mathbf{y},\mathbf{t})}. \end{aligned}$$

where $P_1(\mathbf{y},\mathbf{t}), \dots, P_4(\mathbf{y},\mathbf{t})$ are parametrized as in Equation (14). Gröbner bases [16, § 3.3] let us compute equations vanishing on the image of Ψ_{up}. Here, we ended the

computation early after finding eight relations: six are variables $T_{0,0,0,0}, T_{1,1,1,1}, T_{1,1,1,0}, T_{1,1,0,1}, T_{1,0,1,1}, T_{0,1,1,1,1}$, and the others $f_{\text{up}}(T), g_{\text{up}}(T)$ are homogeneous of degree 5. In fact, these relations generate *all* polynomial constraints on radial quadrifocal tensors—see SM Proposition 6.

5. Solvers

We now describe the construction of our minimal solvers. All solvers use HC to compute solutions to

$$f_1(\mathbf{x}; \mathbf{d}_{\text{target}}) = \cdots = f_N(\mathbf{x}; \mathbf{d}_{\text{target}}) = 0, \qquad (16)$$

where $f_1, \ldots, f_N$ are multivariate polynomial in unknowns $\mathbf{x} \in \mathbb{C}^N$ and given target parameters $\mathbf{d}_{\text{target}} \in \mathbb{R}^M$. For both the general and upright case, we consider an **explicit** formulation where camera matrices are parametrized as in Eq. (5) or Eq. (14), respectively, and an **implicit** formulation using internal constraints described in Section 4.1 or Sec. 4.2. In all cases, we begin with a set of starting parameters $\mathbf{d}_{\text{start}} \in \mathbb{C}^M$ and the algebraically optimal number of starting solutions $\mathbf{x}_1(0), \ldots, \mathbf{x}_d(0) \in \mathbb{C}^N$. These start solutions are precomputed offline using monodromy [18]. The homotopy function used in all cases is given by

$$H(\mathbf{x}; t) = \begin{bmatrix} f_1(\mathbf{x}; (1-t)\mathbf{d}_{\text{start}} + t\mathbf{d}_{\text{target}}) \\ \vdots \\ f_N(\mathbf{x}; (1-t)\mathbf{d}_{\text{start}} + t\mathbf{d}_{\text{target}}) \end{bmatrix} = 0. \qquad (17)$$

Each starting solution $\mathbf{x}_i(0)$ extends uniquely to a solution curve $\mathbf{x}_i(t)$ satisfying $H(\mathbf{x}_i(t); t) = 0$ for all t from 0 to 1, giving solutions to the target system (16) in the limit $t \to 1^-$. Standard numerical predictor/corrector methods allow us to approximate these solution curves. Our implementation is derived from the software `MiNuS` developed in previous work of Fabbri et al. [24]. We refer to the text [73] for further details on solving polynomial systems with HC.

For either of the explicit formulations, $\mathbf{d}_{\text{target}}$ contains the entries of a coefficient matrix expressing the linear constraints on the unknown tensor T in Equation (4). For both implicit formulations, $\mathbf{d}_{\text{target}}$ contains the entries of tensors T_1, T_2, T_3 spanning the nullspace of this coefficient matrix. Thus, the unknown quadrifocal tensor can be written as $T = x_1 T_1 + x_2 T_2 + T_3$, and $N = 2$, $\mathbf{x} = \begin{bmatrix} x_1 & x_2 \end{bmatrix}$. For the general case, we use the system $f_{\text{Nanson}}(T) = g_{\text{Nanson}}(T) = 0$ described in Section 4.1, and in the upright we use $f_{\text{up}}(T) = g_{\text{up}}(T) = 0$.

5.1. 13 pt solver

For either formulation, we start our homotopies from $d = 28$ complex start solutions. In the implicit formulation, we note that although the system defined by two of Nanson's equations has more than 28 complex solutions, any extraneous solutions are not valid quadrifocal tensors and do not need to be tracked. We discard all non-real solutions among the 28 complex target solutions recovered by HC. To recover at most 56 solutions in camera matrices, we apply the map HS defined in Equation (6) when using the explicit formulation ($N = 13$), and solve quadratic equations (see SM Sec. 8 for details) when using the implicit formulation. Having then recovered solutions in uncalibrated cameras, we then perform the metric upgrade in Proposition 1 to recover at most 224 solutions in calibrated cameras. Cameras that do not satisfy chirality constraints [35] may be discarded. From here, it would be possible to recover the 16 sets of Cayley parameters associated to each Euclidean reconstruction. However, this is not necessary, since one solution in a given symmetry class is chiral if and only if they all are—see SM Proposition 4.

5.2. 7 pt upright solver

We start our homotopies with 25 complex start solutions for both formulations, and obtain at most 25 real target solutions. To recover at most 50 solutions in camera matrices, we apply the symmetry $(y_2, y_3, y_4) \mapsto (-y_2, -y_3, -y_4)$ when using the explicit formulation, and for the implicit formulation we solve quadratic equations analagously to the general case. No metric upgrade is necessary.

6. Experiments

Next, we present synthetic and real experiments demonstrating the numerical stability, noise resistance, and practical use of our solvers.

6.1. Synthetic experiments

Numerical stability. To evaluate the numerical stability of the solvers, we generate noiseless instances of the minimal problems with their solutions. We sample n 3D points $\mathbf{X}_k \in \mathbb{R}^3$ from the the uniform distribution over the cube $[-1, 1] \times [-1, 1] \times [1, 3]$, generate 4 upright rotations $\mathbf{R}_j$, and translations $\mathbf{t}_j$, project the point $\mathbf{X}_k$ into camera j as $\mathbf{x}_{jk} = \mathbf{R}_j \mathbf{X}_k + \mathbf{t}_j$, and compute the radial line $\mathbf{l}_{jk}$ passing through point $\mathbf{x}_{jk}$. We fix the coordinate system so that $\mathbf{R}_1 = \mathbf{I}, \mathbf{t}_1 = \mathbf{0}, \mathbf{t}_2 \sim \mathbf{e}_2$.

Let $P_{j,GT}$ be calibrated GT radial cameras, and $P_{j,est}$ calibrated estimated radial cameras. We calculate the tensor error in the Frobenius norm $\|T_{\{P_{j,GT}\}} - T_{\{P_{j,est}\}}\|$, where $T_{\{P_{j,GT}\}}, T_{\{P_{j,est}\}}$ are normalized quadrifocal tensors calculated according to (3). We extract rotations $\mathbf{R}_{j,GT}, \mathbf{R}_{j,est}$ from the radial cameras, and calculate rotation error as $\max_{1 \le i \le 4} \angle \mathbf{R}_{i,GT}{}^T \mathbf{R}_{i,est}$. To measure the translation, we extract the principal axes $\mathbf{p}_{j,GT}$, $\mathbf{p}_{j,est}$, take the shortest distance d_j between $\mathbf{p}_{j,GT}$, and $\mathbf{p}_{j,est}$, and measure the translation error as $\max_{1 \le i \le 4} d_i$. We generated random problem instances and ran the solvers on the noiseless samples until each solver achieved $n = 10000$ successful runs.

Fig. 2 shows histograms of tensor, rotation, and translation errors. All solvers but "13 Implicit" deliver stable

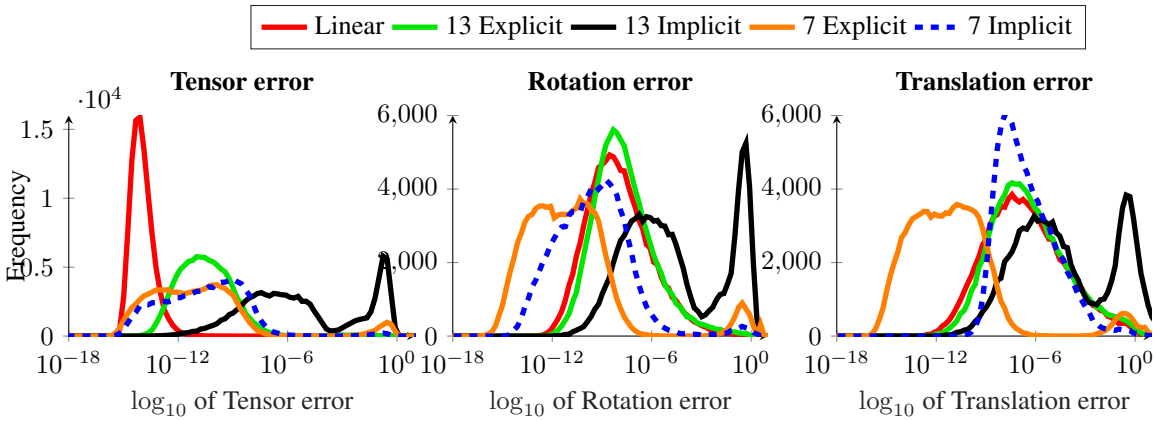

Figure 2. Histogram of $\log_{10}$ tensor, rotation, and translation error of solvers (Tab. 1) computed from 10000 successful noiseless samples. Failure rates for each solver are as follows. Linear: 0.05%, 13 Explicit: 0.20%, 13 Implicit: 29.35%, 7 Explicit: 3.02%, 7 Implicit: 0.27%.

tensors, Fig. 2 (Tensor error), with majority results having errors smaller than 10^{-6}. The performance of "13 Implicit" solver is mixed, with significantly more failures, perhaps due to degree-12 polynomial evaluation. Similarly, Fig. 2 shows rotation and translation errors are also small except for "13 Implicit", peaking below 10^{-6}. The "13 Implicit" solver has, again, mixed bimodal performance with majority of good results but a non-negligible mode of bad results. Hence, we conclude that all solvers but "13 Implicit" are numerically stable for practical use in RANSAC.

Sensitivity to image noise. To investigate the robustness of the solvers to noise, we generate problems as before and perturb the input with noise. Namely, we set the focal length $f = 1000$, and add noise $\frac{\sigma}{f}$ to each projected point $\mathbf{x}_{jk}$. Figure 3 shows errors of the solvers for different values of σ: (i) the performance of minimal solvers degrades gracefully with noise and (ii) all minimal but "13 Implicit" solvers outperform "15 Linear" solver. Interestingly, real experiments presented in Sec. 6.2, show that this instability of "13 Implicit" does not affect its performance in RANSAC.

Sensitivity of upright assumption. To measure the robustness of the 7 point solvers to the deviation α from the upright direction, we perturb noiseless data with upright rotations $\mathbf{R}_j$ generated above by random rotation matrices $\mathbf{R}_{jP}$ with angle α as $\mathbf{R}_j = \mathbf{R}_{jP}\mathbf{R}_j$. Figure 4 shows the errors of the solvers for different values of α: both 7 point solvers provide acceptable performance with more than 40%, resp. 15%, good results at $\alpha = 1°$, resp. $\alpha = 2°$.

6.2. Real experiments

Evaluation in RANSAC. To show how the solvers perform in practice, we employ them within the locally-optimized RANSAC scheme [15]. For the evaluation we consider two datasets containing significant distortion (fisheye lens), *Grossmunster* and *Kirchenge* from Larsson et al. [47]. We also evaluate on 11 scenes from ETH3D [71]. For each dataset we randomly sample 200 sets of 4 images which

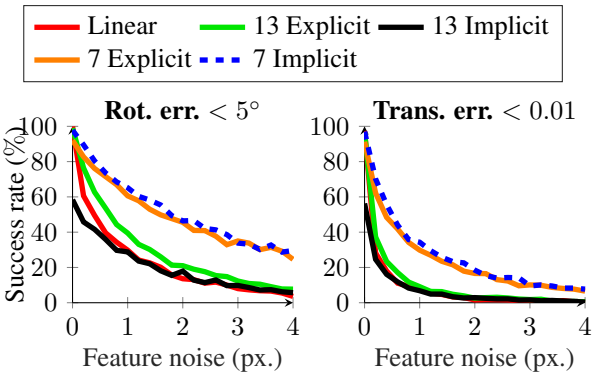

Figure 3. **Noise robustness test.** Percentage of problems, over 10000 runs, of problems whose *left:* rotation, *right:* translation error is below given thresholds, as a function of the feature noise σ. Focal length $f = 1000px$.

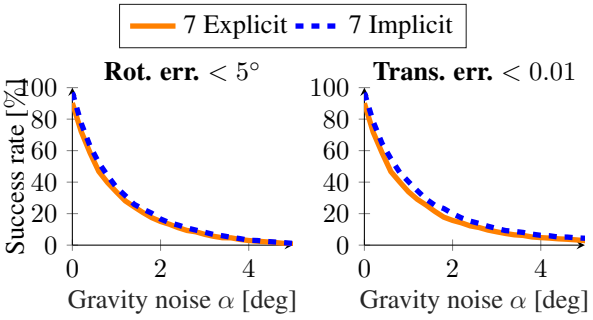

Figure 4. **Upright test** Percentage of problems, over 1000 runs, whose *left:* rotation, *right:* translation error is below given threshold, as a function of deviation α from the upright direction.

share at least 50 3D-points in the ground truth reconstruction. Table 2 shows the success-rate (rotation less than 10° and translation less than $0.25m$) obtained with each solver. Note that only some of the datasets were captured in an *upright* setting, and thus the failure rates for the 7 point solvers vary among the datasets. The 13 point solver has consis-

tently better results than the 15 point linear solver. The 7 point upright solver achieves superior results on scenes where the upright assumption holds. Interestingly, on average, the somewhat unstable "13 Implicit" solver performs slightly better (avg. success rate 0.25) than the second best "13 Explicit" solver (avg. success rate 0.24), leaving the "15 Linear" solver clearly behind (avg. success rate 0.17).

Comparison with Larsson et al. [47]. The authors of [47] present an initialization scheme for radial reconstruction from five images using a trifocal tensor that assumes the principal axes of three cameras intersect, along with a "mixed" trifocal tensor incorporating the other cameras. They also give a detection heuristic for image triplets approximately satisfying the intersecting axes assumption. We replicate their initialization experiment on the Lund Cathedral dataset [62], in which they first generate 1000 potential triplets with intersecting axes and fit radial trifocal tensors via RANSAC. For each of the 100 best triplets, they then select two additional images to use for initialization. Figure 5 compares our method with their initialization scheme using both this heuristic (Right) and with random 5-tuples (Left). After running our method on four images, we triangulate 3D points and register the fifth image. We use bundle adjustment to refine the results of both methods. From the figure, we see that for general data (not necessarily satisfying the intersecting principal axes assumption), our quadrifocal initialization is significantly more accurate. The trifocal method with heuristic triplet-selection, although slightly better than ours, comes at the cost of computing with many more samples. Also, the results indicate the stability of our general method under special motions.

Structure-from-Motion. We integrated our radial quadrifocal tensor solver into the 1D SfM pipeline from Larsson et al. [47], allowing initialization from images in general configuration. Figure 6 shows an example reconstruction from the Kirchenge dataset (369 fisheye images).

7. Conclusion

In summary, our work provides the first minimal solutions for 1D radial camera relative pose in the uncalibrated, calibrated, and upright cases. This resolves an outstanding problem in calibration-free structure-from-motion. Moreover, experiments demonstrate that these solutions yield practical results for 3D reconstruction, and compare favorably to previous work. In RANSAC, the minimal solvers yield more accurate results than the linear solver *on average*, and remain feasible despite the increased runtime. On the theoretical side, we find that these seemingly-difficult problems possess a significant amount of algebraic structure that can be exploited for solving. Since the algebraic degrees of these problems are ultimately only 28 and 25, it is conceivable that more efficient or more stable solutions using existing tools are waiting to be discovered.

All data and software will be made publicly available.

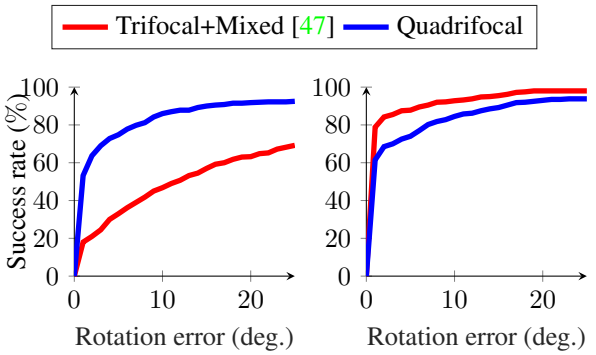

Figure 5. Comparison with trifocal tensor initialization from Larsson et al. [47]. The figure shows the cumulative distribution of the rotation errors. *Left:* Evaluation on randomly selected images. *Right:* Evaluation on images chosen with the heuristic from [47].

Solver	15L	13E	13I	7E	7I
Grossmunster	0.19	**0.27**	0.25	0.06	0.03
Kirchenge	0.19	**0.29**	0.27	0.02	0.01
Courtyard	0.06	0.03	0.04	0.06	**0.07**
Delivery	0.20	0.13	**0.22**	0.18	0.08
Electro	0.16	0.16	0.16	**0.25**	0.13
Facade	0.12	0.09	**0.13**	0.11	0.07
Office	0.17	**0.30**	0.28	0.00	0.07
Pipes	0.38	**0.50**	**0.50**	0.38	0.13
Playground	0.22	**0.26**	**0.26**	0.02	0.03
Relief	0.18	0.29	**0.34**	0.01	0.01
Relief 2	0.14	0.35	**0.37**	0.07	0.06
Terrace	**0.16**	0.14	0.13	0.13	0.11
Terrains	0.24	0.31	0.24	**0.46**	0.39
Average	0.17	0.24	**0.25**	NA	NA

Table 2. **Real tests on datasets [47, 71].** We report the fraction of poses whose rotation error is below 10°, and translation error is below $20cm$. See Sec. 6.2 for more details.

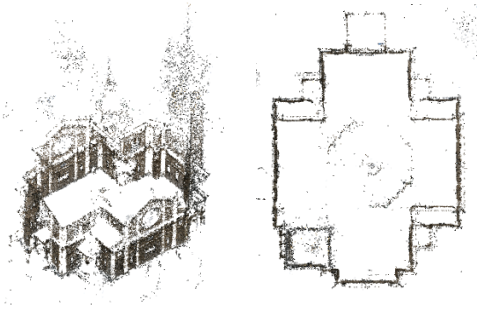

Figure 6. Structure-from-Motion on the Kirchenge [47] dataset.

References

[1] S. Agarwal, N. Snavely, I. Simon, S. M. Seitz, and R. Szeliski, *Building Rome in a day*, IEEE 12th International Conference on Computer Vision, ICCV 2009, Kyoto, Japan, September 27 - October 4, 2009, 2009, pp. 72–79. ↑1

[2] A. A. Ahmadieh and C. Vinzant, *Determinantal representations and the image of the principal minor map*, arXiv 2205.05267, 2022. ↑5

[3] E. Ask, Y. Kuang, and K. Åström, *Exploiting p-fold symmetries for faster polynomial equation solving*, Proceedings of the 21st International Conference on Pattern Recognition, ICPR 2012, Tsukuba, Japan, November 11-15, 2012, 2012, pp. 3232–3235. ↑3

[4] C. Bajaj, *The algebraic degree of geometric optimization problems*, Discrete & Computational Geometry **3** (1988), no. 2, 177–191. ↑3

[5] D. Barath, T. Toth, and L. Hajder, *A minimal solution for two-view focal-length estimation using two affine correspondences*, 2017 IEEE Conference on Computer Vision and Pattern Recognition, CVPR 2017, Honolulu, HI, USA, July 21-26, 2017, 2017, pp. 2557–2565. ↑2

[6] S. Bhayani, Z. Kukelova, and J. Heikkilä, *A Sparse Resultant Based Method for Efficient Minimal Solvers*, 2020 IEEE/CVF conference on computer vision and pattern recognition, CVPR 2020, Seattle, WA, USA, June 13-19, 2020, 2020, pp. 1767–1776. ↑2, 3

[7] A. Borodin and E. M. Rains, *Eynard-Mehta theorem, Schur process, and their Pfaffian analogs*, Journal of Statistical Physics **121** (2005), no. 3-4, 291–317. MR2185331 ↑5

[8] P. Breiding, F. Rydell, E. Shehu, and A. Torres, *Line multiview varieties* (2022). ↑3

[9] P. Breiding and S. Timme, *Homotopycontinuation.jl: A package for homotopy continuation in julia*, Mathematical software – icms 2018, 2018, pp. 458–465. ↑2

[10] T. Brysiewicz, J. I. Rodriguez, F. Sottile, and T. Yahl, *Solving decomposable sparse systems*, Numerical Algorithms (2021). ↑5

[11] M. Byröd, K. Josephson, and K. Åström, *A Column-Pivoting Based Strategy for Monomial Ordering in Numerical Gröbner Basis Calculations*, Computer Vision - ECCV 2008, Marseille, France, October 12-18, 2008, Proceedings, Part IV, 2008, pp. 130–143. ↑2

[12] F. Camposeco, T. Sattler, and M. Pollefeys, *Minimal Solvers for Generalized Pose and Scale Estimation from Two Rays and One Point*, ECCV – European Conference on Computer Vision, 2016, pp. 202–218. ↑2

[13] M. K. Chandraker, S. Agarwal, F. Kahl, D. Nistér, and D. J. Kriegman, *Autocalibration via rank-constrained estimation of the absolute quadric*, 2007 IEEE Computer Society Conference on Computer Vision and Pattern Recognition (CVPR 2007), 18-23 June 2007, Minneapolis, Minnesota, USA, 2007. ↑4

[14] C. Chien, H. Fan, A. Abdelfattah, E. P. Tsigaridas, S. Tomov, and B. B. Kimia, *GPU-based homotopy continuation for minimal problems in computer vision*, IEEE/CVF Conference on Computer Vision and Pattern Recognition, CVPR 2022, New Orleans, LA, USA, June 18-24, 2022, 2022, pp. 15744–15755. ↑3

[15] O. Chum, J. Matas, and J. Kittler, *Locally optimized RANSAC*, Joint Pattern Recognition Symposium, 2003, pp. 236–243. ↑7

[16] D. A. Cox, J. Little, and D. O'Shea, *Ideals, varieties, and algorithms*, 4ed., Undergraduate Texts in Mathematics, Springer, 2015. MR3330490 ↑5, 4

[17] F. Dellaert and A. W. Stroupe, *Linear 2D Localization and Mapping for Single and Multiple Robot Scenarios*, Proceedings of the 2002 IEEE International Conference on Robotics and Automation, ICRA 2002, May 11-15, 2002, Washington, DC, USA, 2002, pp. 688–694. ↑2

[18] T. Duff, C. Hill, A. Jensen, K. Lee, A. Leykin, and J. Sommars, *Solving polynomial systems via homotopy continuation and monodromy*, IMA Journal of Numerical Analysis (2018). ↑4, 6

[19] T. Duff, K. Kohn, A. Leykin, and T. Pajdla, *PLMP - Point-line Minimal Problems in Complete Multi-view Visibility*, 2019 IEEE/CVF International Conference on Computer Vision, ICCV 2019, Seoul, Korea (South), October 27 - November 2, 2019, 2019, pp. 1675–1684. ↑3

[20] ———, *PL_1P - point-line minimal problems under partial visibility in three views*, Computer Vision - ECCV 2020 - 16th European Conference, Glasgow, UK, August 23-28, 2020, Proceedings, Part XXVI, 2020, pp. 175–192. ↑3

[21] T. Duff, V. Korotynskiy, T. Pajdla, and M. H. Regan, *Galois/monodromy groups for decomposing minimal problems in 3D reconstruction*, To appear in SIAM Journal on Applied Algebra and Geometry (2022), available at arXiv2105.04460. ↑3, 2

[22] D. Eisenbud, *Commutative Algebra*, Graduate Texts in Mathematics, vol. 150, Springer-Verlag, New York, 1995. With a view toward algebraic geometry. ↑4

[23] A. Elqursh and A. M. Elgammal, *Line-based relative pose estimation*, The 24th IEEE Conference on Computer Vision and Pattern Recognition, CVPR 2011, Colorado Springs, CO, USA, 20-25 June 2011, 2011, pp. 3049–3056. ↑2

[24] R. Fabbri, T. Duff, H. Fan, M. H. Regan, D. da Costa de Pinho, E. P. Tsigaridas, C. W. Wampler, J. D. Hauenstein, P. J. Giblin, B. B. Kimia, A. Leykin, and T. Pajdla, *TRPLP - Trifocal Relative Pose From Lines at Points*, 2020 IEEE/CVF Conference on Computer Vision and Pattern Recognition, CVPR 2020, Seattle, WA, USA, June 13-19, 2020, 2020, pp. 12070–12080. ↑2, 3, 6

[25] H. Fan, J. Kileel, and B. B. Kimia, *On the Instability of Relative Pose Estimation and RANSAC's Role*, IEEE/CVF Conference on Computer Vision and Pattern Recognition, CVPR 2022, New Orleans, LA, USA, June 18-24, 2022, 2022, pp. 8925–8933. ↑3

[26] O. D. Faugeras, Q. Luong, and S. J. Maybank, *Camera Self-Calibration: Theory and Experiments*, Computer Vision - ECCV'92, Second European Conference on Computer Vision, Santa Margherita Ligure, Italy, May 19-22, 1992, Proceedings, 1992, pp. 321–334. ↑2

[27] O. D. Faugeras, L. Quan, and P. F. Sturm, *Self-Calibration of a 1D Projective Camera and its Application to the self-calibration of a 2D projective camera*, IEEE Transactions on Pattern Analysis and Machine Intelligence **22** (2000), no. 10, 1179–1185. ↑2

[28] M. A. Fischler and R. C. Bolles, *Random sample consensus: a paradigm for model fitting with applications to image analysis and automated cartography*, Communications of the ACM **24** (1981), no. 6, 381–395. ↑3

[29] F. Fraundorfer, P. Tanskanen, and M. Pollefeys, *A Minimal Case Solution to the Calibrated Relative Pose Problem for the Case of Two Known Orientation Angles*, Computer Vision - ECCV 2010, 11th European Conference on Computer Vision, Heraklion, Crete, Greece, September 5-11, 2010, Proceedings, Part IV, 2010, pp. 269–282. ↑2

[30] D. R. Grayson and M. E. Stillman, *Macaulay2, a software system for research in algebraic geometry*. Available at http://www.math.uiuc.edu/Macaulay2/. ↑2, 4

[31] R. Hartley and F. Schaffalitzky, *Reconstruction from projections using Grassmann tensors*, Computer Vision - ECCV 2004, 2004, pp. 363–375. ↑2

[32] ———, *Reconstruction from projections using Grassmann tensors*, International Journal of Computer Vision **83** (2009), no. 3, 274–293 (English). ↑2, 4, 5

[33] R. Hartley and A. Zisserman, *Multiple view geometry in Computer Vision*, Second, Cambridge University Press, Cambridge, 2003. With a foreword by Olivier Faugeras. ↑1, 2, 4

[34] R. I. Hartley, *In Defence of the 8-Point Algorithm*, Procedings of the Fifth International Conference on Computer Vision (ICCV 95), Massachusetts Institute of Technology, Cambridge, Massachusetts, USA, June 20-23, 1995, 1995, pp. 1064–1070. ↑2

[35] ———, *Chirality*, International Journal of Computer Vision **26** (1998), no. 1, 41–61. ↑6, 3

[36] J. D. Hauenstein and M. H. Regan, *Adaptive strategies for solving parameterized systems using homotopy continuation*, Applied Mathematics and Computation **332** (2018), 19–34. MR3788668 ↑3

[37] J. D. Hauenstein, J. I. Rodriguez, and F. Sottile, *Numerical computation of galois groups*, Foundations of Computational Mathematics **18** (2018), no. 4, 867–890. ↑3

[38] O. Hesse, *Die cubische Gleichung, von welcher die Lösung des Problems der Homographie von M. Chasles abhängt*, Journal für die Reine und Angewandte Mathematik **62** (1863), 188–192. MR1579236 ↑2

[39] O. Holtz and B. Sturmfels, *Hyperdeterminantal relations among symmetric principal minors*, Journal of Algebra **316** (2007), no. 2, 634–648. ↑2, 5, 3

[40] P. Hruby, T. Duff, A. Leykin, and T. Pajdla, *Learning to solve hard minimal problems*, IEEE/CVF Conference on Computer Vision and Pattern Recognition, CVPR 2022, New Orleans, LA, USA, June 18-24, 2022, 2022, pp. 5522–5532. ↑2, 3, 5

[41] H. Huang and L. Oeding, *Symmetrization of principal minors and cycle-sums*, Linear Multilinear Algebra **65** (2017), no. 6, 1194–1219. MR3615538 ↑5

[42] J. Kileel, *Minimal problems for the calibrated trifocal variety*, SIAM Journal on Applied Algebra and Geometry **1** (2017), no. 1, 575–598. MR3705779 ↑3

[43] L. Kneip, R. Siegwart, and M. Pollefeys, *Finding the exact rotation between two images independently of the translation*, ECCV – European Conference on Computer Vision, 2012, pp. 696–709. ↑2

[44] Z. Kukelova, M. Bujnak, and T. Pajdla, *Automatic generator of minimal problem solvers*, ECCV – European Conference on Computer Vision, 2008. ↑2

[45] V. Larsson and K. Åström, *Uncovering symmetries in polynomial systems*, European Conference on Computer Vision, 2016, pp. 252–267. ↑3

[46] V. Larsson, M. Oskarsson, K. Åström, A. Wallis, Z. Kukelova, and T. Pajdla, *Beyond Gröbner Bases: Basis Selection for Minimal Solvers*, 2018 IEEE Conference on Computer Vision and Pattern Recognition, CVPR 2018, Salt Lake City, UT, USA, June 18-22, 2018, 2018, pp. 3945–3954. ↑3

[47] V. Larsson, N. Zobernig, K. Taskin, and M. Pollefeys, *Calibration-free structure-from-motion with calibrated radial trifocal tensors*, European Conference on Computer Vision, 2020, pp. 382–399. ↑2, 3, 4, 7, 8, 6

[48] S. Lin and B. Sturmfels, *Polynomial relations among principal minors of a 4× 4-matrix*, Journal of Algebra **322** (2009), no. 11, 4121–4131. ↑2, 5

[49] M. Liu, C. Pradalier, and R. Siegwart, *Visual homing from scale with an uncalibrated omnidirectional camera*, IEEE Transactions on Robotics **29** (2013), no. 6, 1353–1365. ↑2

[50] E. Martyushev, J. Vráblíková, and T. Pajdla, *Optimizing elimination templates by greedy parameter search*, IEEE/CVF Conference on Computer Vision and Pattern Recognition, CVPR 2022, New Orleans, LA, USA, June 18-24, 2022, 2022, pp. 15733–15743. ↑3

[51] P. Miraldo, T. Dias, and S. Ramalingam, *A Minimal Closed-Form Solution for Multi-perspective Pose Estimation using Points and Lines*, Computer Vision - ECCV 2018 - 15th European Conference, Munich, Germany, September 8-14, 2018, Proceedings, Part XVI, 2018, pp. 490–507. ↑2

[52] P. Moulon, P. Monasse, and R. Marlet, *Global fusion of relative motions for robust, accurate and scalable structure from motion*, IEEE International Conference on Computer Vision, ICCV 2013, Sydney, Australia, December 1-8, 2013, 2013, pp. 3248–3255. ↑1

[53] T. Muir, *The relations between the coaxial minors of a determinant of the fourth order*, Transactions of The Royal Society of Edinburgh **39** (1900), no. 2, 323–339. ↑2, 5

[54] R. Mur-Artal, J. M. M. Montiel, and J. D. Tardós, *ORB-SLAM: A versatile and accurate monocular SLAM system*, IEEE Transactions on Robotics **31** (2015), no. 5, 1147–1163. ↑1

[55] E. Nanson, *On the relations between the coaxial minors of a determinant*, The London, Edinburgh, and Dublin Philosophical Magazine and Journal of Science **44** (1897), no. 269, 362–367. ↑2, 5

[56] D. Nistér, *An efficient solution to the five-point relative pose problem*, IEEE Transactions on Pattern Analysis and Machine Intelligence **26** (June 2004), no. 6, 756–770. ↑2

[57] D. Nister, R. Hartley, and H. Stewénius, *Using Galois Theory to Prove Structure from Motion Algorithms are Optimal*, 2007 IEEE Conference on Computer Vision and Pattern Recognition, 2007, pp. 1–8. ↑3, 2

[58] D. Nistér, *An efficient solution to the five-point relative pose problem*, IEEE Transactions on Pattern Analysis and Machine Intelligence **26** (2004), no. 6, 756–777. ↑2

[59] L. Oeding, *The quadrifocal variety*, Linear Algebra and its Applications **512** (2017), 306 –330. arxiv 1501.01266. ↑2

[60] L. Oeding, *Set-theoretic defining equations of the variety of principal minors of symmetric matrices*, Algebra and Number Theory **5** (2011), no. 1, 75–109. MR2833786 ↑5

[61] L. Oeding and S. V. Sam, *Equations for the fifth secant variety of Segre products of projective spaces*, Experimental Mathematics **25** (2016), no. 1, 94–99. MR3424836 ↑4

[62] C. Olsson and O. Enqvist, *Stable structure from motion for unordered image collections*, Scandinavian Conference on Image Analysis, 2011. ↑8, 7

[63] C. Olsson, V. Larsson, and F. Kahl, *A quasiconvex formulation for radial cameras*, IEEE conference on computer vision and pattern recognition, CVPR 2021, virtual, june 19-25, 2021, 2021, pp. 14576–14585. ↑3

[64] J. Pritts, Z. Kukelova, V. Larsson, Y. Lochman, and O. Chum, *Minimal solvers for rectifying from radially-distorted scales and change of scales*, International Journal of Computer Vision **128** (2020), no. 4, 950–968. ↑2

[65] L. Quan, *Two-Way Ambiguity in 2D Projective Reconstruction from Three Uncalibrated 1D Images*, IEEE Transactions on Pattern Analysis and Machine Intelligence **23** (2001), no. 2, 212–216. ↑2, 4

[66] L. Quan and T. Kanade, *Affine structure from line correspondences with uncalibrated affine cameras*, IEEE Transactions on Pattern Analysis and Machine Intelligence **19** (1997), no. 8, 834–845. ↑2

[67] R. Raguram, O. Chum, M. Pollefeys, J. Matas, and J. -M. Frahm, *USAC: A universal framework for random sample consensus*, IEEE Transactions on Pattern Analysis Machine Intelligence **35** (2013), no. 8, 2022–2038. ↑3

[68] S. Ramalingam and P. F. Sturm, *Minimal Solutions for Generic Imaging Models*, CVPR – IEEE Conference on Computer Vision and Pattern Recognition, 2008. ↑2

[69] C. Sagüés, A. C. Murillo, J. J. Guerrero, T. Goedemé, T. Tuytelaars, and L. V. Gool, *Localization with omnidirectional images using the radial trifocal tensor*, Proceedings of the 2006 IEEE International Conference on Robotics and Automation, ICRA 2006, May 15-19, 2006, Orlando, Florida, USA, 2006, pp. 551–556. ↑2

[70] J. L. Schönberger and J.-M. Frahm, *Structure-from-motion revisited*, Conference on Computer Vision and Pattern Recognition (CVPR), 2016. ↑1

[71] T. Schops, J. L. Schonberger, S. Galliani, T. Sattler, K. Schindler, M. Pollefeys, and A. Geiger, *A Multi-View Stereo Benchmark With High-Resolution Images and Multi-Camera Videos*, Proceedings IEEE Conference on Computer Vision and Pattern Recognition (CVPR) 2017, 2017. ↑7, 8, 6

[72] A. Shashua and L. Wolf, *On the structure and properties of the quadrifocal tensor*, Computer Vision - ECCV 2000, 2000, pp. 710–724 (English). ↑2

[73] A. J. Sommese and C. W. Wampler II, *The numerical solution of systems of polynomials arising in engineering and science*, World Scientific, Hackensack, NJ, 2005. MR2160078 ↑3, 6

[74] F. Sottile and T. Yahl, *Galois groups in enumerative geometry and applications*, arXiv, 2021. ↑2

[75] S. Thirthala and M. Pollefeys, *Radial multi-focal tensors*, International Journal of Computer Vision **96** (2012), no. 2, 195–211 (English). ↑2, 3

[76] S. Thirthala and M. Pollefeys, *The Radial Trifocal tensor: a Tool for Calibrating the Radial Distortion of Wide-Angle Cameras*, 2005 IEEE Computer Society Conference on Computer Vision and Pattern recognition (CVPR 2005), 20-26 June 2005, San Diego, CA, USA, 2005, pp. 321–328. ↑2

[77] B. Triggs, *Autocalibration and the absolute quadric*, Proceedings of IEEE Computer Society Conference on Computer Vision and Pattern Recognition, 1997, pp. 609–614. ↑4

[78] R. Y. Tsai, *A versatile camera calibration technique for high-accuracy 3D machine vision metrology using off-the-shelf TV cameras and lenses*, IEEE Journal on Robotics and Automation **3** (1987), no. 4, 323–344. ↑2

[79] J. Ventura, C. Arth, and V. Lepetit, *An efficient minimal solution for multi-camera motion*, Proceedings of the IEEE International Conference on Computer Vision (ICCV), 2015, pp. 747–755. ↑2